VIBFAT – VIBRATION-INDUCED FATIGUE LIFE ESTIMATION OF THE VERTICAL TAIL OF THE F/A-18 AIRCRAFT USING VIRTUAL SENSING

Vesa Nieminen[1], Tomi Viitanen, Keijo Koski, Risto Laakso and Mikko Savolainen

[1] VTT Technical Research Centre of Finland Ltd, Tietotie 4C, FI-02150 Espoo, Finland; vesa.nieminen@vtt.fi

Abstract: Unmeasured quantities and responses at selected locations in structural monitoring can be estimated by different virtual sensing techniques. Virtual sensing enables estimation of operational response of the structure at any location based on a limited set of measurements and the numerical model of the structure. This paper presents the study for expansion of sparse response data by means of a component simulation model to enable fatigue analysis anywhere in the structural component or subassembly under question.

The object of this case study is a high-performance F/A-18 Hornet fighter aircraft. It is extremely manoeuvrable thus capable of flying at high angles-of-attack. In those flight regimes the high-energy vortices generated by the inner wing leading edge extensions induce severe cyclic loading to the downstream structure by exciting the resonance frequencies of the empennage. The broad band dynamic loads, i.e. buffet loads, together with the static manoeuvring loads, contribute to the fatigue of the Vertical Tails (VT) of the aircraft. The Finnish Air Force (FINAF) has been running the Hornet Operational Loads Measurement (HOLM) program since 2006 to quantify the effects of operational usage on the structure of the F/A-18C/D aircraft. The HOLM program employs two intensively instrumented aircraft without operational restrictions. Both Vertical Tails of the HOLM aircraft include three strain sensors at the Vertical Tail Stubs and two acceleration transducers at the tip of the Vertical Tail, enabling to detect all the significant loading events locally in the VT.

The virtual sensing applied in this study is based on bandpass filtering the measured acceleration data to get modal-specific responses for the primary VT modes. Component FE-model of the VT is then used to create modal-specific acceleration-to-strain conversion functions for the structural details of interest. For each mode individual virtual strain signal will be generated at the chosen structural location. All the signals of the primary modes at the same location are combined by the superposition principle to achieve the total virtual strain, which then can be used as an input in the typical fatigue analyses.

Research focus of this study is applicability of the local/component FE-models for the virtual sensing. Research question is to investigate the limitations of the method when applying only a local/component FE-model and minimum number of sensors for the virtual sensing. The results demonstrated applicability of the local component FE-model and only a single acceleration measurement for virtual sensing in cases where dominant modes are well separated.

Keywords: Virtual sensing, vibration, fatigue, Vertical Tail, HOLM

INTRODUCTION

Unmeasured quantities and responses at locations in structural monitoring can be estimated by different virtual sensing techniques. Virtual sensing enables estimation of operational response of the structure at any location based on a limited set of measurements and the numerical model of the structure. This paper presents the study for expansion of sparse response data by means of simulation model to enable fatigue analysis anywhere in the structural component under question.

Research focus of this study is applicability of the local/component FE-models for virtual sensing in cases where global FE-model is not available. The modelling effort for the component or subassembly of the structure only is naturally significantly smaller compared with the global model of the whole assembly. Research question is to investigate the limitations of the method when applying only local/component FE-model and minimum number of sensors for the virtual sensing. In this case only one sensor was needed.

Dynamic loading environment

High-performance fighter aircraft, like the F/A-18 Hornet, is extremely manoeuvrable thus capable of flying at high angles-of-attack, too. In those flight regimes the high-energy vortices from by the inner wing leading edge extensions (LEX) generate additional lift, but as a drawback, induce severe cyclic loading to the downstream structure by exciting the resonance frequencies of the empennage (Figure 1). The broad band dynamic loads, i.e. buffet loads, together with the static manoeuvring loads, contribute to the fatigue of the Vertical Tails (VT) of the aircraft. The Vertical Tail first bending mode has a significant impact on the fatigue life of the lower aft root region, especially the fuselage to the VT attachment frames. The Vertical Tail first torsion mode predominantly affects the life of the upper region of the structure [1].

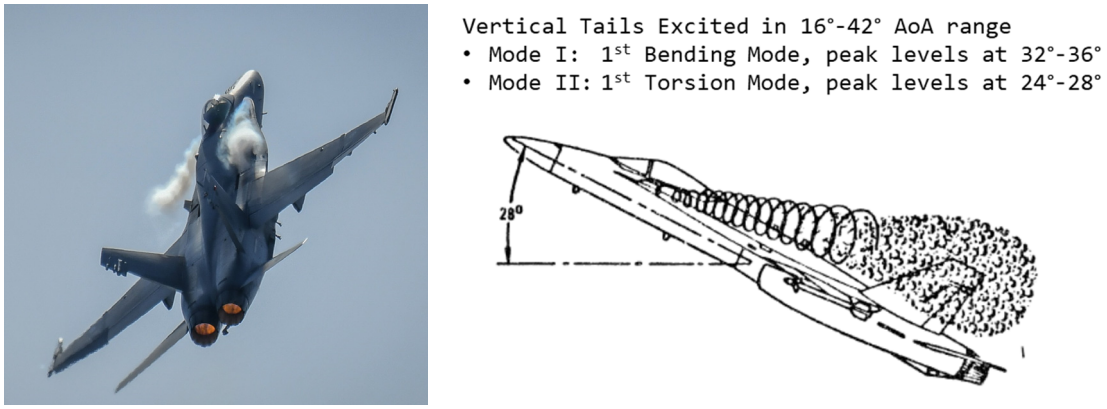

Figure 1. High-energy vortices generated by the inner wing leading edge extensions resulting regions of very low pressure that condenses the water vapor of the air (left figure: courtesy of the FINAF) and induce severe cyclic loading to the downstream structure, like Vertical Tails, by exciting the resonance frequencies of the empennage (right figure, edited from Ref. [1]).

The F/A-18 Vertical Tail structure

The Vertical Tail structure comprises a multispar main structural box extending from the 22.5 % spar to the 77.5 % spar and from the lower closing rib to the upper closing rib. The face sheets are multi-directional carbon fiber-reinforced polymer (CFRP) composite laminates. The VT structure is connected to the aft fuselage by six attachment frames, so called stubs, forming a highly redundant structure (Figure 2). The attachment stubs have an I-beam cross-sectional geometry.

In the structures of the aircraft where high vibrations are present, repeated loads can cause the fasteners to loosen, allowing very small cyclic displacements to occur between the two contacting surfaces. It has

been a common knowledge among the F/A-18 operators' that the extrinsic signs of fatigue in the Vertical Tail, i.e. the black smears from the fasteners and loose fasteners are due to fretting[1].

The Hornet Operational Loads Measurement system

The Finnish Air Force has been running the Hornet Operational Loads Measurement (HOLM) program since 2006 to quantify the effects of operational usage on the structure of the F/A-18C/D aircraft, and thus to support the aircraft structural integrity management efforts. The HOLM program encompasses two intensively instrumented aircraft without operational restrictions.

The HOLM system divides into onboard and ground systems, having a Compact Flash (CF) memory card as a data link between them. The onboard system consists of Data Acquisition Units (DAU) and instrumentation with 44 strain sensors and 4 acceleration transducers, fitted on globally and locally significant structural locations. The optimized sampling rates of the strains vary from 1.280 Hz in the highly vibrating locations (such as VT) to 640 Hz elsewhere. The accelerations are sampled at 2.560 Hz. Both Vertical Tails of the HOLM aircraft include strain sensors at three VT stubs and two acceleration transducers at the tip of the VT, enabling to detect all the significant loading events of the structure. In addition to the structural responses, more than 250 flight parameters have simultaneously been recorded from the standard data buses of the aircraft. The ground system involves equipment, hardware and software, by which the recorded data from the onboard system can be upgraded to e.g., fatigue lives and various kind of distribution summaries.

The HOLM sensors discussed in this paper are: A06, a Brüel&Kjær 4570-D DC response accelerometer, having a measuring range of ±500 G, and strain sensor S73a which is a Vishay Micro-Measurements EA-13-125PC-350/W dual-pattern strain gage, having a strain range of ±5 %.

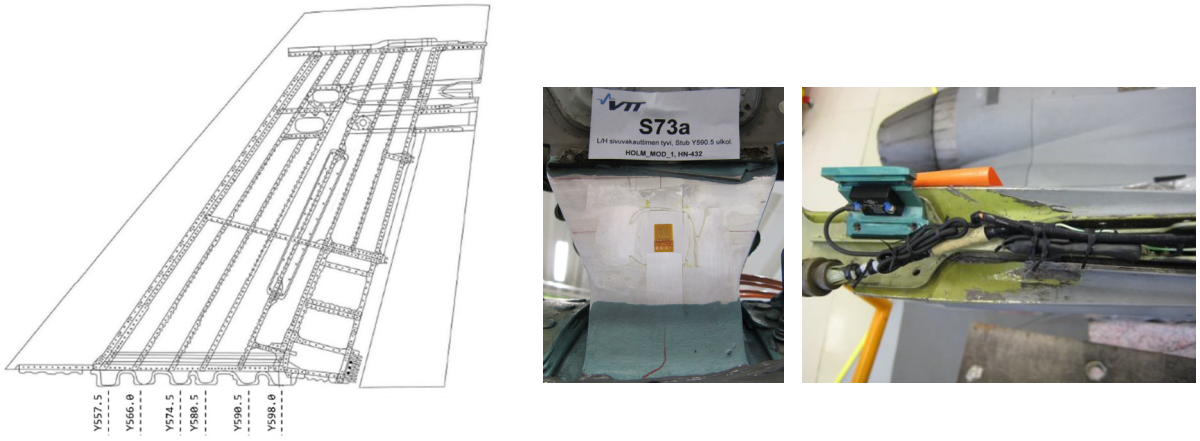

Figure 2. The Vertical Tail structure highlighting the six attachment frames (left), the location of the strain sensor S73a (middle, Y590.5), and the acceleration transducer A06 (right).

The measured HOLM data has been summarized in various ways over the years, including the breakdown of the calculated fatigue damage between the maneuver-induced quasi-static loading and the buffeting-induced stochastic loading. As illustrated in Figure 3, fatigue damage proportion from the buffet loading is relatively high in the aft fuselage, up to 96 %.

[1] Fretting is the application of oscillating tangential forces to two nominally clamped free surfaces. Although the surfaces may appear to be stationary with respect to one another, sections move relative to one another, creating regions of microslip – and when subjected to repeated loads can cause the initiation and propagation of fatigue cracks. [2]

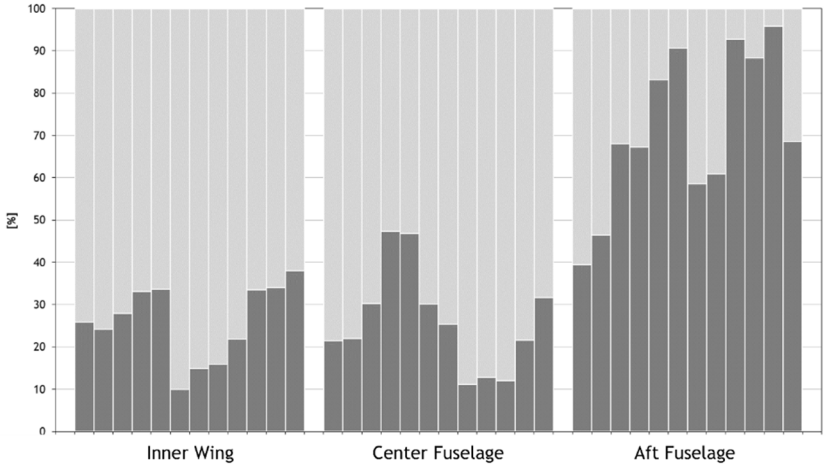

Figure 3. The fatigue damage breakdown between the maneuver-induced quasi-static loading (light bars) and the buffeting-induced stochastic loading (dark bars) in the subassemblies of the F/A-18C HOLM aircraft. Each bar represents an analysis location of interest and includes results from numerous flights.

METHODOLOGY

In cases where dominant modes are well separated in frequency range of interest, the following straightforward method based on bandpass filtering can be applied for virtual sensing. This method enables application of virtual sensing with only one sensor. In more complicated cases where the dominant modes are not well separated, additional sensors are generally needed and modal contributions of different modes during operation can be estimated, e.g., by least squares method [3].

Modal expansion approach

The idea is to utilize acceleration measurements from limited number of locations and a dynamic model of the subassembly to obtain virtual strain – and thus calculate life estimation – at unmeasured location(s). In this case FE-model of the VT structure only was applied for virtual sensing. The goal is to investigate applicability and limitations of the local/component FE-model and single sensors for the virtual sensing.

This paper presents the work for expansion of sparse response data by means of simulation model to enable fatigue analysis anywhere in the structure under question. This is done by bandpass filtering the measured acceleration data to get modal-specific responses for the primary VT modes. Local component FE model of the VT is then used to create modal specific displacement-to-strain conversion factors for the critical locations of interest. For each mode individual virtual strain signal will be generated at the chosen structural location. All the signals of the primary modes are combined by the superposition principle to achieve the total virtual strain, which then can be used as an input in the typical fatigue analyses. The procedure is suitable in cases where the structures are primarily experiencing intense dynamic loadings. The approach is illustrated in Figure 4.

Measured acceleration signal is first converted into displacement signal using time domain integration twice. At each step before the integration, it is necessary to remove DC-component and eliminate high-frequency noise from the signal. The resulting displacement signal is then band-pass filtered into bandwidths of interest, here: 5-10 Hz, 10-20 Hz, and 40-50 Hz. By modal-specific conversion factors provided by the FEA, displacement signals are converted into virtual strain signals, and after summing up, a combined virtual strain is resulted. After constructing the virtual strain, strain time history can be simplified as a collection of turning points from which the strain cycles can be counted by traditional Rainflow algorithm [5] for the fatigue damage analysis.

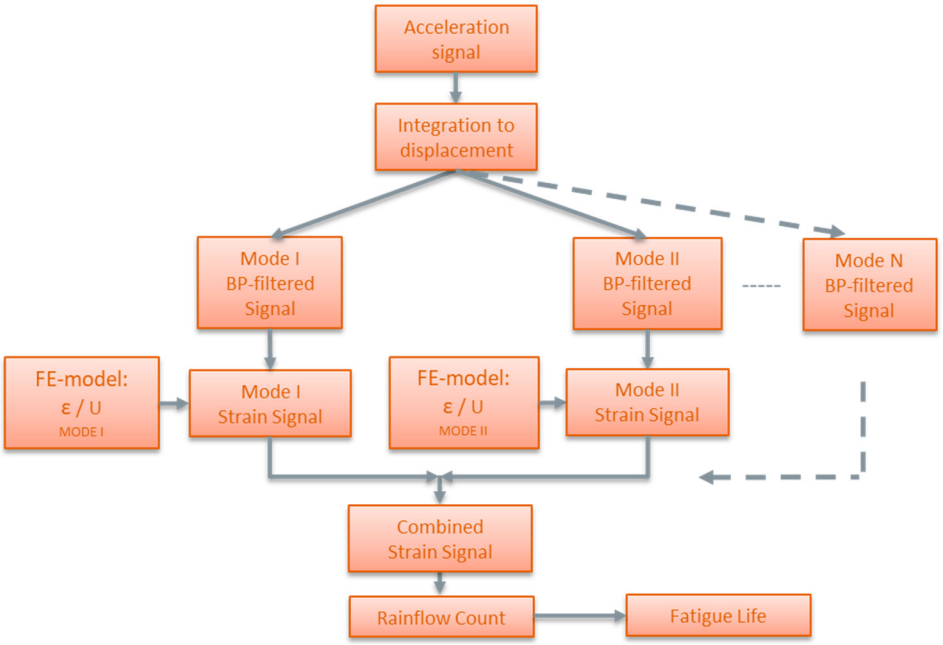

Figure 4. The analysis process for obtaining the virtual strain signal and fatigue life.

Local/Component FE model

The FE model of the VT and its support structure included one quarter of the left aft fuselage. Quarter of the aft fuselage was longitudinally limited near the outermost stub sections (Figure 5). The model was fully fixed at cutting edges of the aft fuselage. The FE model mainly consisted of linear shell elements, added with beam elements as stiffeners and solid elements in some areas, depending on the modeled structure. Most of the VT outer surfaces consisted of composite structures having anisotropy etc. in the shell element sections. The stubs were initially modeled with the shell elements. To improve the strain calculation accuracy, the instrumented stub Y590.5 was modeled with the solid elements. The original FE models were provided by Patria.

The structural FE-mesh of the VT and its support structure eventually consisted of 295059 nodes and 198981 elements.

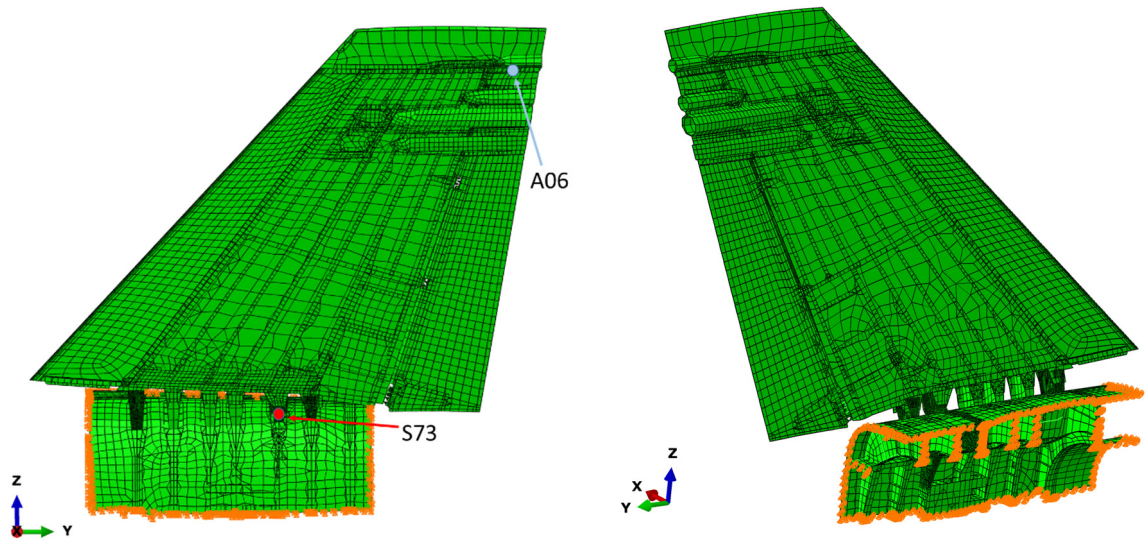

Figure 5. The FE model of the VT. Boundary condition locations are shown in orange. The locations of the acceleration transducer A06 and the strain gage S73a have been emphasized.

Once the FE model of the VT and its support structure had been constructed, the natural frequencies and the corresponding mode shapes were calculated by Lanczos method in ABAQUS/Standard. The eigenvalues were calculated up to 100 Hz. As a result, the natural frequencies, corresponding modal testing condition of the structure, were: 14.93 Hz for the 1st bending mode (Mode 1), and 45.15 Hz for the 1st torsional mode (Mode 2). Modal displacements at the acceleration transducer A06 location and modal strains at the strain sensor S73a location were calculated. Their relation formed the foundation for the virtual sensing. The FE model dynamics was validated in more detail by comparison with experimental modal analysis results presented in the subsequent section.

MODEL VALIDATION

Experimental modal analysis

To validate the FE model of the VT and its support structure and to evaluate model expansion capabilities for a single accelerometer data, vibration characteristics of the aircraft were identified experimentally. To identify vibration characteristics of the aircraft, lowest elastic natural modes of the VT, i.e. natural frequencies, modal damping factors and mode shapes were determined experimentally by modal testing [4]. To identify global mode shape characteristic of the aircraft, measurement points were located also to other parts of the aircraft, see Figure 6. Totally 50 acceleration response points were measured, all locations in three directions. Special focus was put on the modes around about 15 Hz and 45 Hz. As mentioned earlier, the VT experiences high vibration levels at about these frequencies due to flow-induced excitations [1].

The VT (LH and RH side) was excited by an instrumented impact hammer having a soft plastic tip. Traditional impact testing and random impact excitation for Operational Modal Analysis (OMA) was used to identify the modal parameters [4]. Random impact excitation technique for Operational Modal Analysis was demonstrated to be applicable for identification of very closely spaced modes.

Identified modes are presented in Table 1. Identified modal damping factors are also shown in the table. Due to symmetry of the structure, each main VT modes (modes at about 15 Hz and 45 Hz) are divided into two modes having close natural frequencies: symmetric and antimetric modes. To quantify orthogonality or independency of identified mode shapes, AutoMAC criterion was applied, see the last column of Table 1. Modal Assurance Criterion (MAC) is a measure of the degree of similarity or correlation of two modal vectors. The elements of the MAC matrix (j,k) for the modal vectors $\boldsymbol{\phi}_j$ and $\boldsymbol{\phi}_k$ are defined as (Eqn. 1):

$$\boldsymbol{MAC_{jk}} = \frac{\left(\boldsymbol{\phi}_j{}^T \boldsymbol{\phi}_k\right)^2}{\left(\boldsymbol{\phi}_j{}^T \boldsymbol{\phi}_j\right)\left(\boldsymbol{\phi}_k{}^T \boldsymbol{\phi}_k\right)} \tag{1}$$

MAC takes values between 0 and 1; values closer to 0 indicate that those vectors are orthogonal, while the closer to 1 indicates high correlation. It is evident that the measurement mesh is not enough extensive to identify properly the lowest global mode shapes of the aircraft (modes at 8.96 Hz and 9.65 Hz) resulting spatial aliasing, and therefore the MAC values are high between these modes. However, the focus in this study was on the VT modes and the diagonals are quite low between these modes.

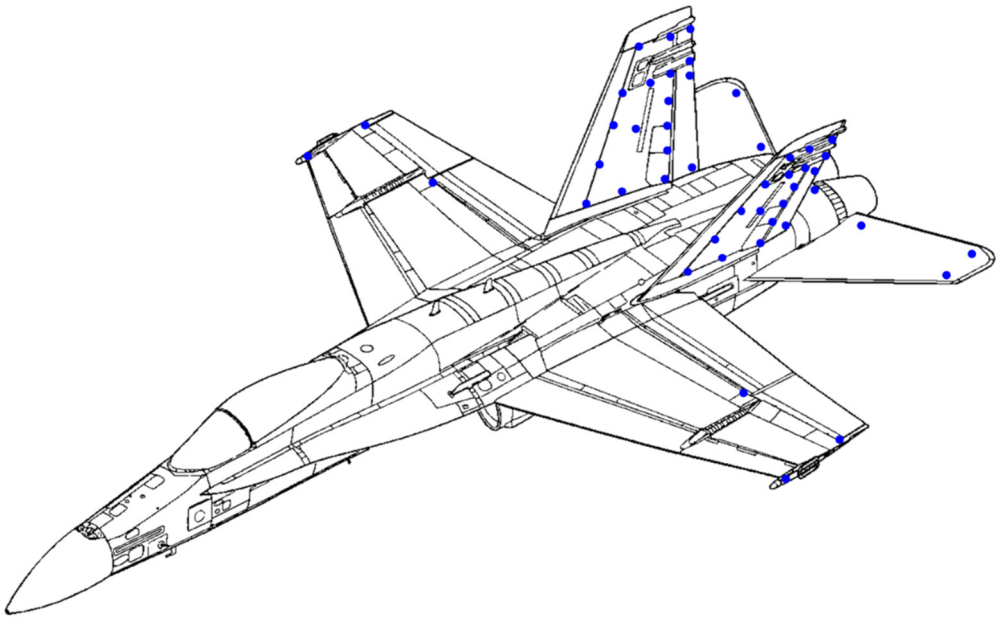

Figure 6. The measurement points in the experimental modal analysis. A total of 50 measurement points were used.

Table *1*. The experimentally identified modes and the AutoMAC matrix of the identified mode shapes.

Mode no	Freq [Hz]	Damp [%]	Description	AutoMAC
1	8.96	1.0	Global torsional	
2	9.65	2.4	Global torsional+roll	
3	13.75	1.9	HT bending, out of phase	
4	**15.15**	**1.3**	**First VT+HT bending, antimetric, VTs in phase**	
5	**15.66**	**0.5**	**First VT bending, symmetric, VTs out of phase**	
6	22.13	3.1	Tail twisting	
7	*23.80*	*17.2*	*RH Rudder rotation?*	
8	*30.93*	*8.1*	*LH Rudder rotation?*	
9	**45.91**	**1.2**	**VT torsion, symmetric**	
10	**45.95**	**0.8**	**VT torsion, antimetric**	
11	62.15	4.1	LH VT 2. bending	
12	62.92	4.9	RH VT 2. bending	
13	84.41	2.9	RH Rudder torsion	
14	86.24	2.5	LH Rudder torsion	

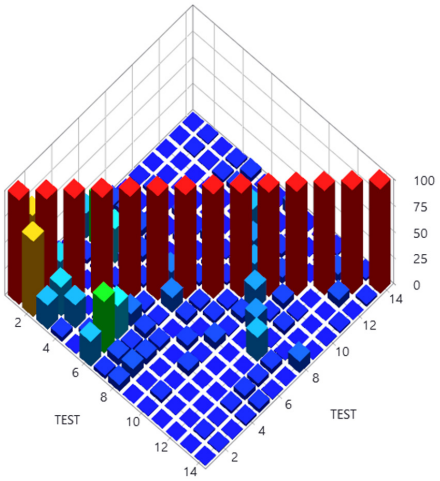

FE-model validation

Eigenvalues and eigenvectors calculated by the FE-model are shown in Table 2. Correlations between numerical and experimental modes are presented in Table 3 and corresponding MAC matrix between experimental and calculated mode shapes is shown in Figure 7. Due to spatial aliasing, calculated lowest VT bending and torsion modes have high MAC values with several experimental modes. Table 3 shows that the FE-model predicts relatively acceptable the first symmetric bending and first torsional modes of the VT (rows 5 and 9); differences in terms of natural frequencies are not very high and MAC values are higher than 95%. Mode shape comparisons for these modes are presented in Figure 8 and Figure 9.

For corresponding antimetric modes the MAC values are slightly lower, but still higher than 90 %. It is evident, that the component model cannot simulate global modes of the aircraft and therefore correlation for the other modes is significantly worse as can be seen in Table 3.

The MAC matrix presented in Figure 7 indicates correlation of the first calculated bending mode also with lower elastic modes. These comparisons are also included in Table 3; comparisons in first three rows marked in red are artificial which means that the compared mode shapes are not the same in these cases and they do not correspond to each other. However, because the local FE-model cannot simulate these lowest modes, best which one could try to do is to estimate these three lowest modes by the first calculated bending FE-mode and use this first FE-mode in modal expansion process for the frequency range of these lowest modes. As an example, a mode shape comparison for experimental global torsional mode at 8.9 Hz versus numerical first VT bending mode at 14.9 Hz (MAC 73.4) is presented in Figure 10. This experimental global torsional mode induces slightly rigid body movement for the VT, which the component FE-model cannot simulate, resulting low MAC value. It is evident that this estimation introduces error for this frequency band, because the MAC values presented in first three rows in Table 3 are rather low. The goal of this case study was to investigate amount of this induced error for the virtual sensing. It is assumed that amount of the error introduced can be roughly predicted by considering the MAC value between the real experimental mode shape and the numerical mode shape applied into the particular bandwidth.

Table *2*. The calculated natural modes.

Mode	Frequency	Description
1	14.93	**First VT bending**
2	31.46	*Rudder rotation*
3	45.15	**VT torsion**
4	55.93	VT 2. bending
5	64.67	VT longitudinal bending
6	77.78	Rudder + VT torsion

Table *3*. Correlation of numerical and experimental modes (EMA refers to Experimental Modal Analysis). Rows marked in red are artificial; compared mode shapes are not the same in these cases and they do not correspond each other.

#	FEA	Hz	EMA	Hz	Freq. Diff. (%)	MAC (%)	Description
1	1	14.93	1	8.96	-	73.4	Global torsional
2	1	14.93	2	9.65	-	83.4	Global torsional+roll
3	1	14.93	3	13.75	-	92.6	HT bending, out of phase
4	1	14.93	4	15.15	-1.4	98.6	First VT+HT bending, antimetric, VTs in phase
5	**1**	**14.93**	**5**	**15.66**	**-4.7**	**99.2**	**First VT bending, symmetric, VTs out of phase**
6	1	14.93	6	22.13	-	73.9	Tail twisting
7	1	14.93	*7*	*23.80*	-	67.4	*RH Rudder rotation?*
8	2	31.46	8	30.93	1.7	77.1	*LH Rudder rotation?*
9	**3**	**45.15**	**9**	**45.91**	**-1.7**	**96.0**	**VT torsion, symmetric**
10	3	45.15	10	45.95	-1.8	93.0	VT torsion, antimetric
11	4	55.93	11	62.15	-10.0	88.1	LH VT 2. bending
12	6	77.78	14	86.24	-9.8	62.9	LH Rudder torsion

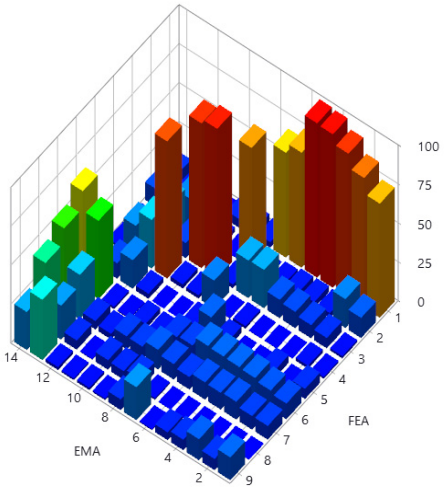

Figure 7. MAC comparison of experimental and calculated mode shapes.

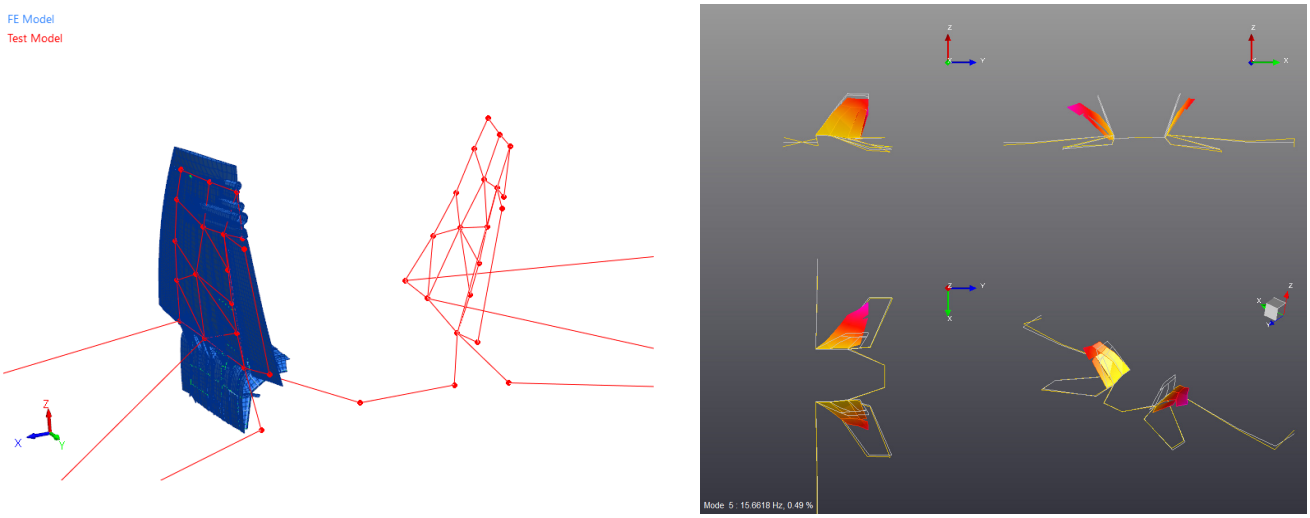

Figure 8. Comparison of experimental and numerical mode shapes; first VT bending mode at 15.7 Hz (symmetric) (MAC 99.2). Experimentally identified mode shape is shown in the right.

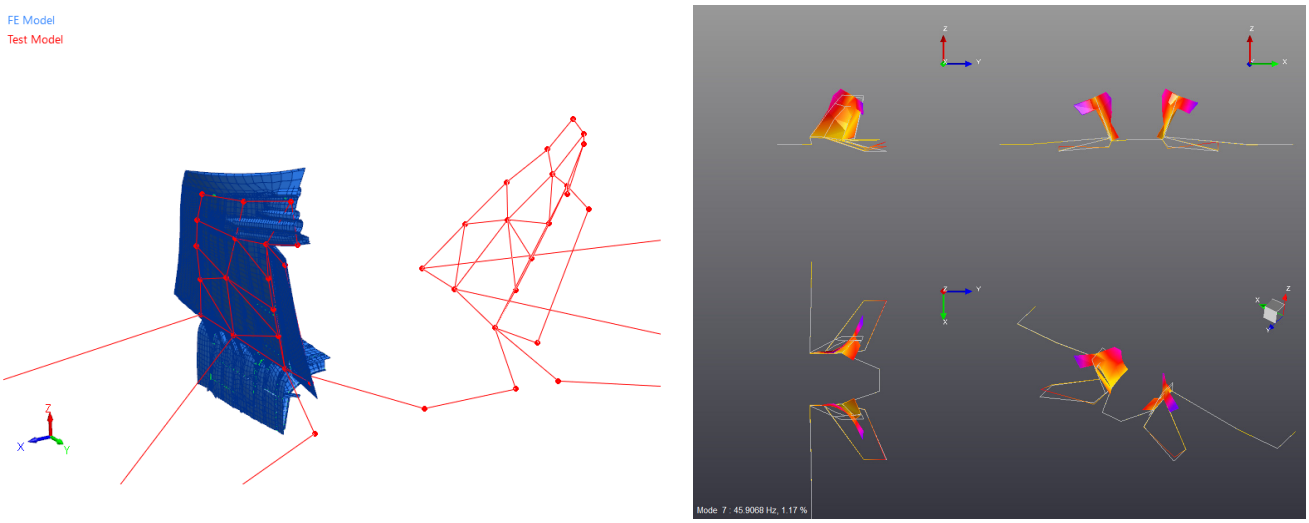

Figure 9. Comparison of experimental and numerical mode shapes; first VT torsion mode at 45.9 Hz (symmetric) (MAC 96.0). Experimentally identified mode shape at 45.91 Hz is shown in the right.

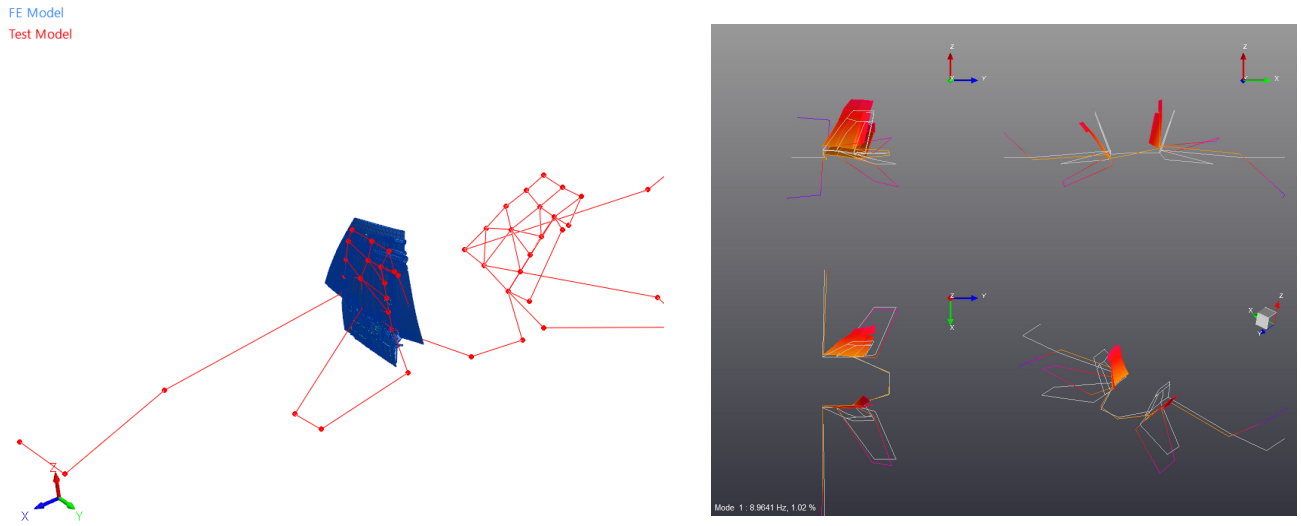

Figure *10*. Comparison of experimental and numerical mode shapes; experimental global torsional mode at 8.9 Hz vs numerical first VT bending mode at 14.9 Hz (MAC 73.4). Experimentally identified mode shape shown in the right reveals global torsional behaviour of the aft of the fuselage.

PROOF-OF-CONCEPT TEST CASE

The constructed proof-of-concept model was tested with the recorded signals from an example flight. Selected set of flight parameters are presented in Figure 11. It can be noted that the flight includes a decent amount of maneuvering resulting maximum accelerations in the region of ±140 G in the aft tip of the Vertical Tail.

The autospectra for the recorded acceleration and strain signals averaged over the example flight are presented in Figure 12. The DC-component of these signals has been removed by band-pass filtering (3-256 Hz). The acceleration spectrum integrated into displacement is also shown in the figure. Spectra show significant resonance peaks at 15.2 Hz and at 45.9 Hz, which equal to the 1st bending and 1st torsional modes of the VT at operating condition. The resonance peaks at 8.75 Hz corresponds the global torsional mode. Frequency of this peak is slightly different compared with the modal testing result, which is probably caused by different boundary conditions during operation. These resonance peaks can also be seen in the strain spectrum and therefore these seem to be the most significant response components of the VT in fatigue point of view.

The bandwidths of interest in virtual sensing which were used for the band-pass filtering of the displacement signal were determined based on these most significant resonance ranges. Bandwidths for the 1st bending and 1st torsional modes were 10-20 Hz and 40-50 Hz, respectively. In addition, for resonance at 8.75 Hz, a separate bandwidth of 5-10 Hz was applied. As mentioned in the previous chapter, strain-displacement factor of the first calculated bending mode was used also for this bandwidth.

Examples of time history comparisons between the constructed virtual strain and measured strain in different bandwidths are presented in Figure 13. The total summed virtual strain with respect to the measured strain (including DC-component) are also shown in the figure. The figure shows satisfactory overall correlation of virtual strains for the bandwidth of 10-20 Hz and 40-50 Hz. Main source of the error of the reconstructed response for these main modes is probably lower MAC correlation of the antimetric modes, see Table 3. For 5-10 Hz bandwidth, the estimation error caused by inaccurate FE-mode shape used can also be detected.

Comparison of averaged autospectra of the reconstructed strain and the measured strain signal S73a is presented in Figure 14. Highest difference can be detected at 8.75 Hz which corresponds to the global

torsional mode. As expected, the reconstructed strain at this mode has been exaggerated, because this global torsional mode induces slightly rigid body movement for the VT, which the component FE-model cannot simulate.

After constructing the virtual strain, strain time history (variable amplitude signal) was simplified as a collection of constant amplitude cycles, peak-valley pairs, from which the strain cycles were counted by Rainflow algorithm [5]. The representative fatigue damage analysis could be done by the traditional stress-life, SN method, assuming linear-elastic material behaviour and thus by replacing the stress with strain. By representative SN curve (in this case 7050_PLATE, Kt=3.0 [6]) the strain amplitudes can be related to the number of cycles to failure. It should be noted that the used method utilized strain amplitudes so that the maximum stress in the given SN curve was converted into equivalent strain range assuming linear-elastic response of the material ($S_{max} = E \cdot 2 \cdot \varepsilon_a/(1-R)$), and mean strain correction for the non-DC-components of the time history was not needed. The fatigue damage of the period could be evaluated by Miner's cumulative fatigue damage rule which states that the fatigue damage fraction is equal to the ratio of the number of cycles at a given strain level to the fatigue life in cycles at the same strain level. The reference location in the analysis was selected just as an example and did not represent a fatigue critical location. Therefore, the last step of the process presented here include the Rainflow counting comparison supported by a commonly used SN-curve.

Fatigue life can be approximated by the Eqn. 2. The number of cycles to failure N_f are presented as a function of strain amplitude (ε_a) and stress or strain ratio (R):

$$N_f(\varepsilon_a, R) = \frac{10^{10.0}}{\left(\frac{2E\varepsilon_a}{1-R} \cdot (1-R)^{0.64}\right)^{3.96}} \tag{2}$$

where E is the Young's Modulus.

The Rainflow counting was done having an amplitude bin width of 27.5 µm/m. With the selected representative SN-curve, the ratio of the calculated cumulative fatigue damage between the constructed virtual strain and the measured strain was approx. 9 %, i.e. the results are very close to each other.

Comparison of Rainflow count histograms from the example flight between the virtual strain and the unfiltered measured strain signals is presented in Figure 15. The representative SN-curve approximated as Eqn. 2 is also presented as a reference. Some differences can be observed at high strain amplitude bins, but overall correlation of the Rainflow count can be considered satisfactory.

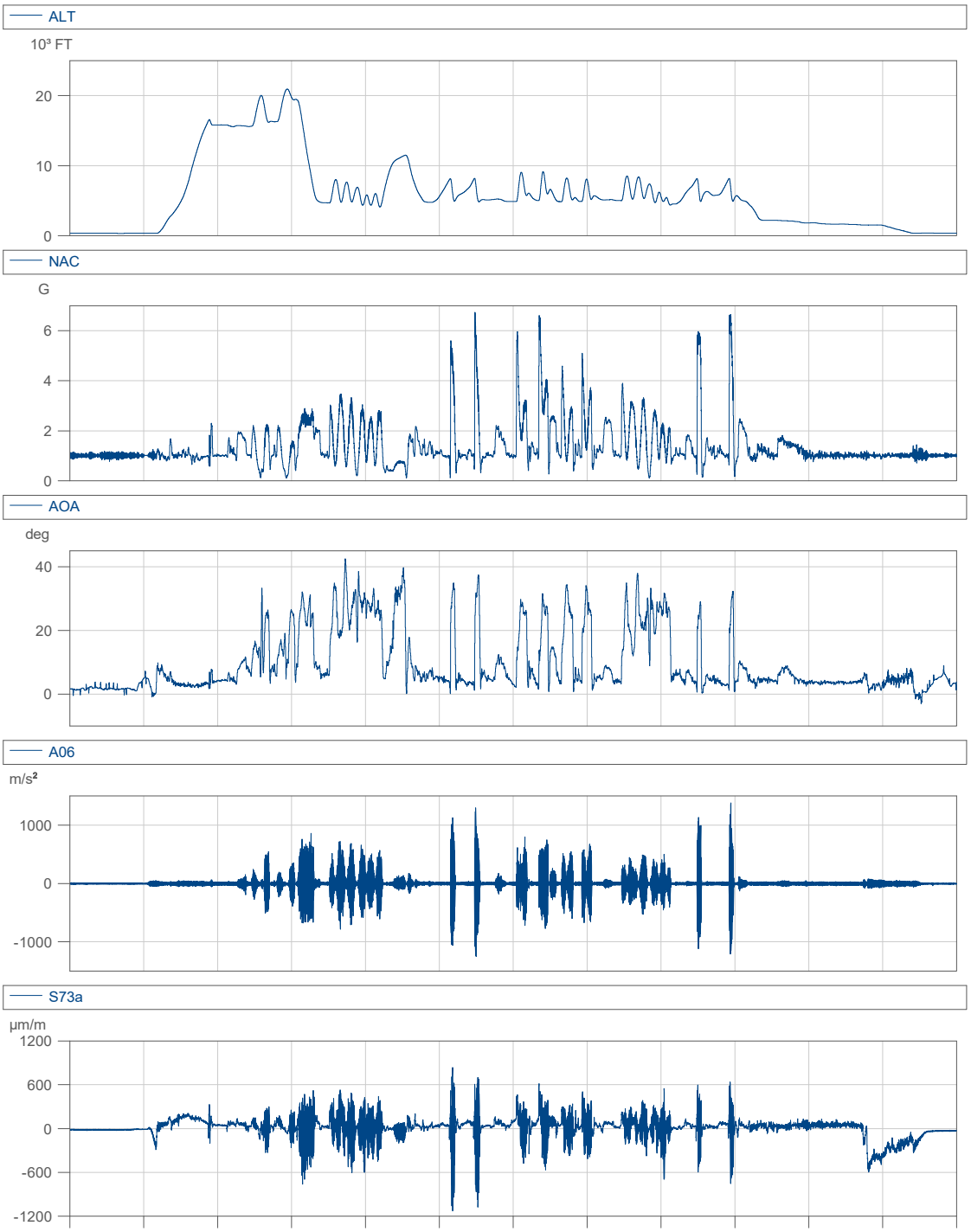

Figure 11. Selected time histories from the example flight. Signals from top to bottom are ALT: Altitude, NAC: Normal acceleration, AOA: Angle of Attack, A06: Vertical Tail acceleration, S73a: Vertical Tail strain. The time on the x-axis is intentionally cropped due to confidentiality reasons.

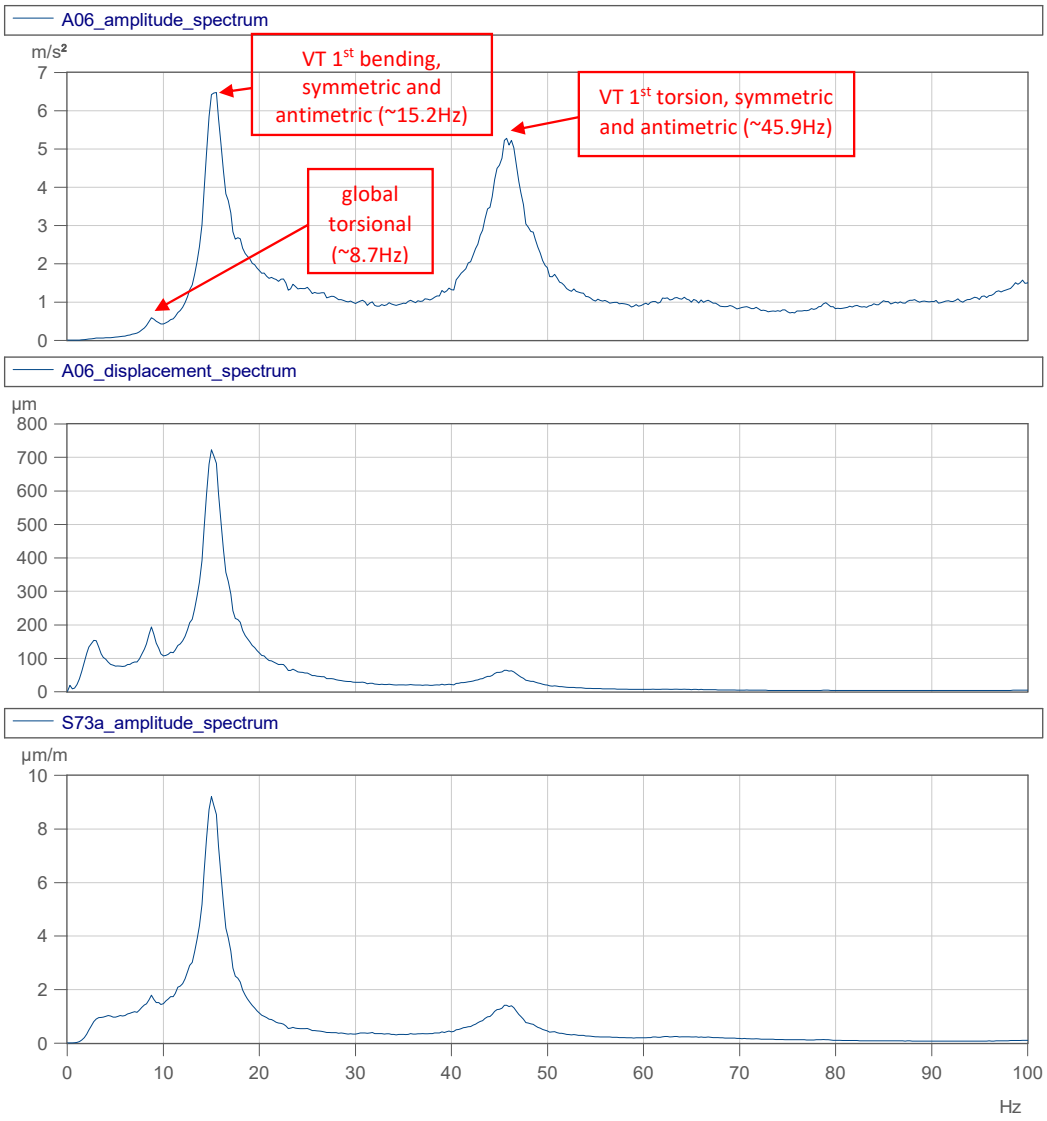

Figure 12. The amplitude and displacement spectra of the acceleration signal A06, and the amplitude spectrum of the strain signal S73a in the frequency range 0-100 Hz. (Frequency resolution of the spectra was 0.25 Hz)

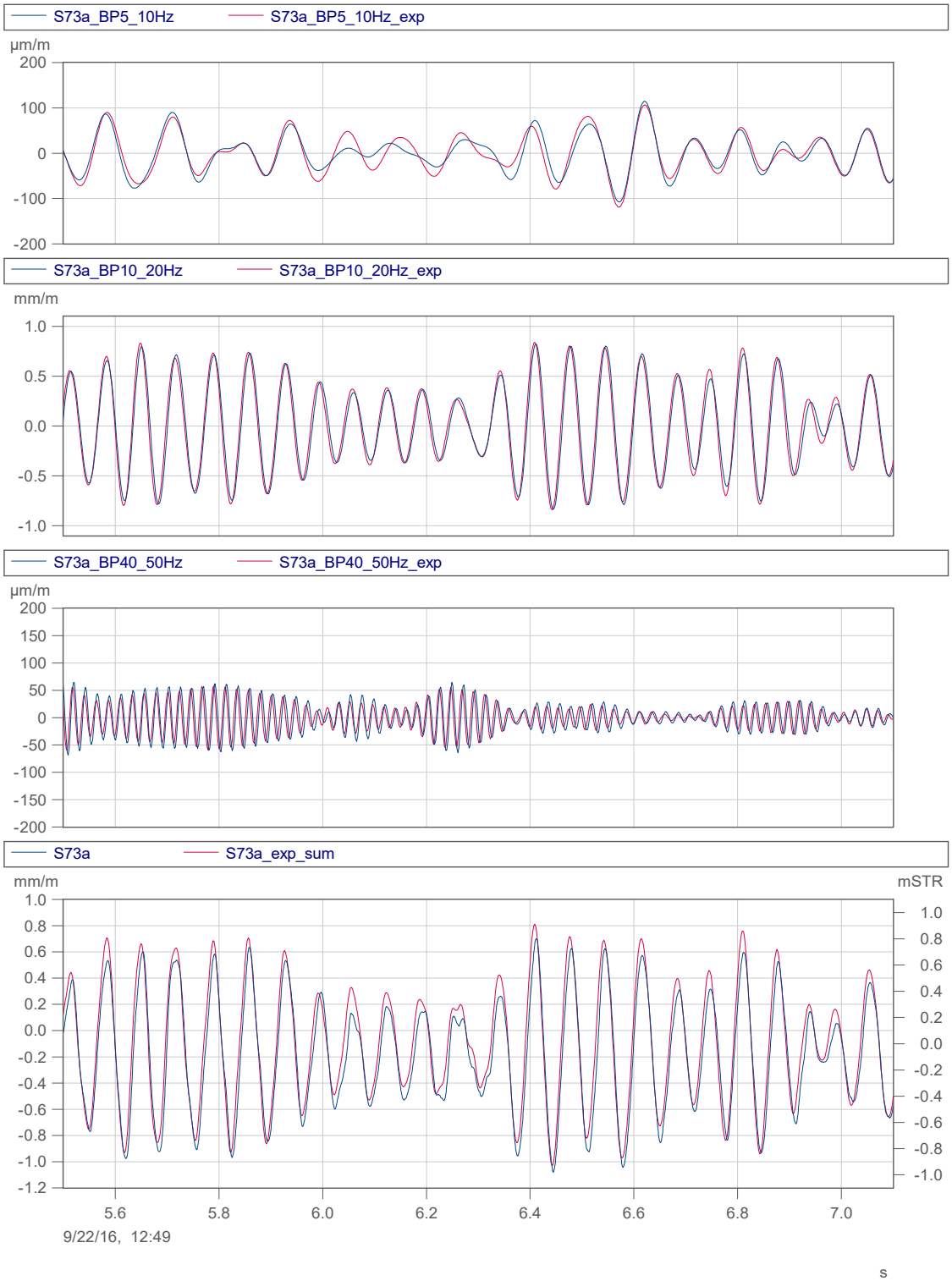

Figure 13. A time history comparison between the virtual strain (_exp suffix) and the measured strain in the bandwidths (from top to bottom) of 5-10 Hz, 10-20 Hz, 40-50 Hz, and full bandwidth. The bottom figure represents the summed components of the virtual strain with respect to the measured strain (including the DC-component also). It can be noted that the measured strain signal includes a slight delay originated from different anti-alias filtering compared with the acceleration measurement channel.

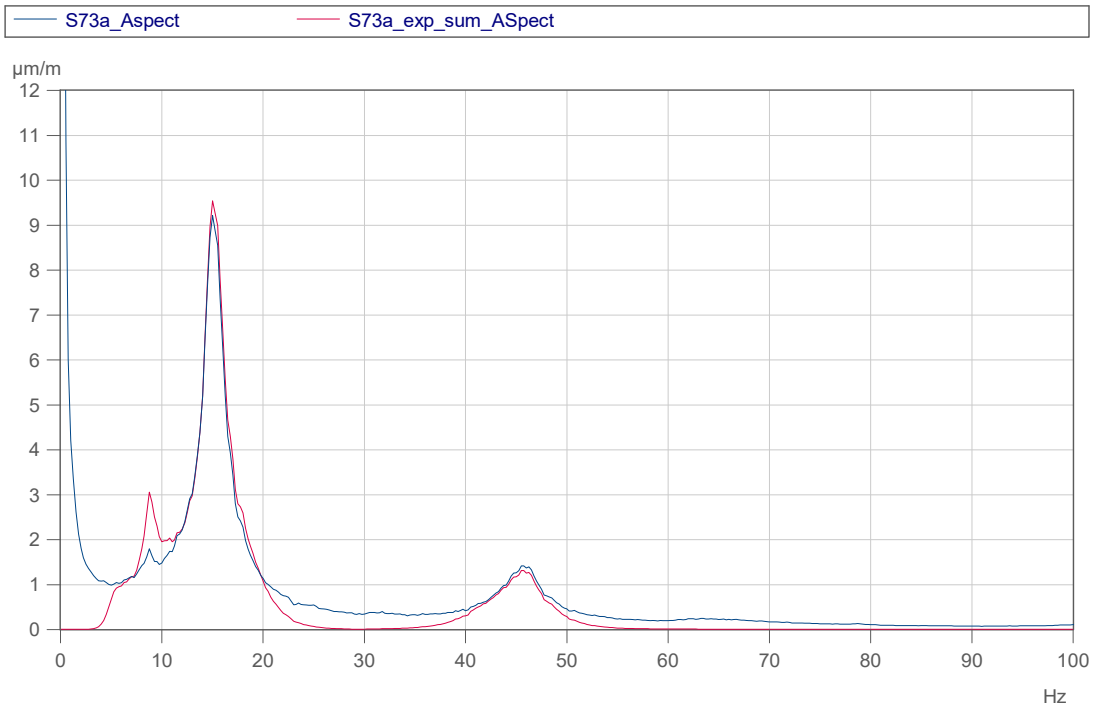

Figure 14. The averaged autospectra of the measured strain signal S73a (blue) and the corresponding reconstructed strain (red).

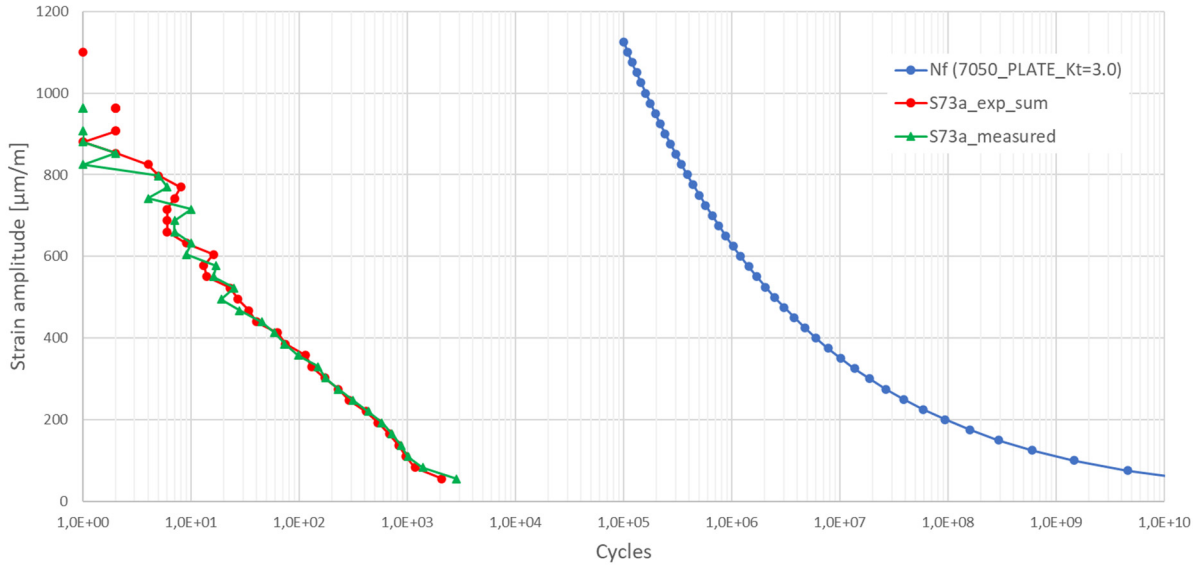

Figure 15. Rainflow count histograms (bin width 27.5 µm/m) from the example flight between the virtual strain (_exp_sum suffix) and unfiltered measured strain signals. The representative SN-curve (7050_PLATE_Kt=3.0, R = -1) approximated as Eqn. 2 is presented as a reference.

CONCLUSIONS

Satisfactory overall correlation of virtual strains with the measured ones for the bandwidths 10-20 Hz and 40-50 Hz were achieved for the reference location of the VT. Main source of the error of the reconstructed response for these main modes is probably lower MAC correlation of the antimetric modes. For 5-10 Hz bandwidth, the estimation error caused by inaccurate FE-mode shape used was slightly larger. However, considering inaccuracies due to limitations of the component FE-model, the overall accuracy of this virtual sensing method can be considered satisfactory in this case.

First VT bending mode is the major contributor for the fatigue life of the Vertical Tail root region. An obvious shortcoming of the method is the exclusion of the steady-state conditions, i.e. the method is most efficient in cases where the dynamical loading is the major contributor for the fatigue of the structure. However, comparison of Rainflow counts indicated that in this example case contribution of the ignored steady-state responses for the fatigue of VT is not very significant.

The results demonstrated applicability of local component FE-model and only a single acceleration measurement for virtual sensing in cases where dominant modes are well separated. However, limitations of the component model should be checked, e.g., by MAC correlation analysis for each dominant mode.

REFERENCES

[1] Conser, D.P., Graham, A.D., Smith, C.J. and Yule, C.L. (1996), *The Application of Dynamic Loads to a Full-Scale F/A-18 Fatigue Test Article*, ICAS Proceedings 1996, Volume 2, Paper ICAS-96.5.10.5, pp. 2465-2480, 20th Congress of the International Council of the Aeronautical Sciences (ICAS), Sorrento, Napoli, Italy, 8-13 September, 1996, ISBN 1-56347-219-8.

[2] Birch, P.R. (1998), A Study of Fretting Fatigue in Aircraft Components, Master of Science Thesis in Materials Science and Engineering, Massachusetts Institute of Technology, USA.

[3] Nieminen V. and Sopanen J. (2023), *Optimal sensor placement of triaxial accelerometers for modal expansion,* Mechanical Systems and Signal Processing, vol. 184, 2023.

[4] Nieminen V. (2023), *Modal Testing of Vertical Tail of F/A-18 Hornet*, Proceedings of the 31st symposium of ICAF - the International Committee on Aeronautical Fatigue and Structural Integrity, Delft, 26-29 June 2023.

[5] ASTM E1049-85 (Reapproved 2011), *Standard Practices for Cycle Counting in Fatigue Analysis*, ASTM International, West Conshohocken, PA, United States.

[6] Rice, R.C., Jackson, J.L., Bakuckas, J. and Thompson, S. (2003), Metallic Materials Properties Development and Standardization (MMPDS), Report No. DOT/FAA/AR-MMPDS-01, U.S. Department of Transportation, Federal Aviation Administration (FAA), Washington, DC, USA.